American Mineralogist, Volume 75, pages 1029–1042, 1990

Experimental biotite-quartz melting in the KMASH-CO_2 system and the role of CO_2 in the petrogenesis of granites and related rocks

JONATHAN W. PETERSON,* ROBERT C. NEWTON
Department of the Geophysical Sciences, University of Chicago, 5734 South Ellis Avenue, Chicago, Illinois 60637, U.S.A.

ABSTRACT

Melting relations of biotite + quartz + feldspar assemblages were investigated experimentally in the system K_2O-MgO-Al_2O_3-SiO_2-H_2O-CO_2 (KMASH-CO_2). At pressures above ~2.5 kbar, melting of phlogopite + quartz and phlogopite + quartz + sanidine assemblages in the presence of equimolar H_2O-CO_2 fluids occurs at temperatures as low as, or even lower than, in the presence of pure H_2O fluid. The melting temperature of phlogopite + quartz + sanidine under equimolar fluids decreases to 700 °C or even lower with increasing pressure above 6 kbar. The data suggest but do not prove a melting minimum, with molar $CO_2/(CO_2 + H_2O)$ of the liquid as high as 0.4. This contrasts with the small solubility of CO_2 in haplogranitic liquids, and is likely caused by high solubility of a $MgCO_3$ complex. Therefore, the minimum liquid is richer in mafic components and CO_2 than most granites. Vapor-saturated melting (molar $H_2O/CO_2 = 1$) of phlogopite + quartz to enstatite + liquid was determined by reversed experiments to occur between 740 and 770 °C at 3.5 kbar, ~30 °C lower than in the pure-H_2O system. Near-solidus liquids of this reaction may be initially somewhat metastable because of delayed enstatite growth or resorption. At 2.5 kbar, the incongruent melting of phlogopite + quartz + sanidine to enstatite + liquid occurs between 757° and 773 °C at fluid compositions of molar $H_2O/(CO_2 + H_2O)$ between 0.39 and 0.27, based on reversed determinations.

Our results indicate a more significant role of CO_2 in granitic and charnockitic magmas than commonly realized. Low-temperature residual liquids of syenitic to lamprophyric composition are possible, and this may explain the close association of granite plutons and calc-alkaline lamprophyres. Evolution of CO_2 upon crystallization of charnockitic magmas in the deep crust may cause granulite metamorphism of surrounding country rocks. Differentiation of the crust in incompatible elements may be facilitated by CO_2-rich mafic anatectic liquids.

INTRODUCTION

Experimental studies of rock melting, particularly those involving the volatile component H_2O, have had significant influence on the investigation of crustal processes. The demonstration that the melting points of feldspar (Goranson, 1938), quartz (Kennedy et al., 1962), and simple granite-analogue assemblages (Tuttle and Bowen, 1958) are lowered with elevated H_2O pressures has swung opinion away from the subsolidus metasomatic theory of the origin of granite to a magmatic interpretation. It is now known that many common rock compositions melt in the presence of a free H_2O fluid phase at pressure and temperature conditions attainable during periods of high-grade crustal mobilization (see Wyllie, 1977), such as orogenic and rifting events. A number of recent experimental studies have also shown that vapor-absent melting of rocks containing hydrous minerals, principally biotite, yields granitic liquids in the upper part of the high-grade metamorphic temperature range (750–900 °C: Le Breton and Thompson, 1988; Vielzeuf and Holloway, 1988; Peterson and Newton, 1989).

The role of the volatile component CO_2 in melting of the crust has not been as thoroughly investigated as that of H_2O. Preliminary experimental studies indicate only a small solubility of CO_2 in granitic melts (e.g., Kadik and Lukanin, 1973), leading some investigators (e.g., Holloway, 1976) to suggest a rather minor chemical role for CO_2, but rather more of a mechanical effect in granite crystallization, by virtue of continuous vapor saturation. More recently, Grant (1986), arguing on the basis of the experimental work of Wendlandt (1981), assigned a more important chemical role to CO_2. Wendlandt's work indicated a much lower melting point for biotite granite in the presence of CO_2-rich fluids than did earlier studies (e.g., Novgorodov and Shkodzinskiy, 1974). At present the role of CO_2 in magmas is still a subject of debate, with unresolved differences existing among experimental studies.

Figure 1 is a P-T diagram illustrating melting equilibria

* Present address: Amoco Production Company, P.O. Box 3092, Houston, Texas 77253, U.S.A.

0003–004X/90/0910–1029$02.00

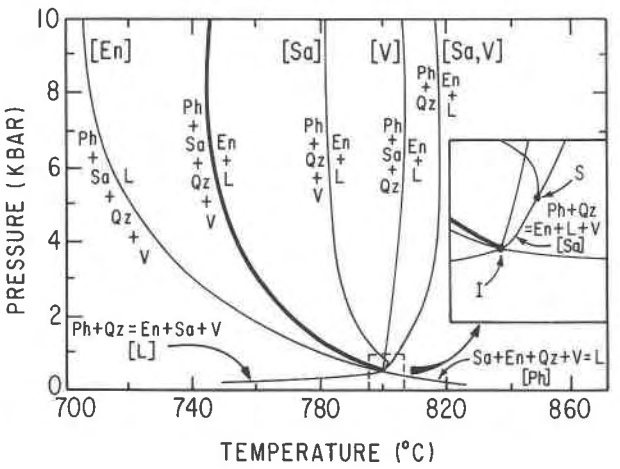

Fig. 1. Univariant equilibria in the KMASH and KMASH-CO_2 (bold curve) systems, from Peterson and Newton (1989) and Wendlandt (1981), respectively. Abbreviations: Ph = phlogopite; Sa = sanidine; En = enstatite; Qz = quartz; L = liquid; V = vapor. Curves are designated by brackets enclosing a phase or phases not participating in equilibria. Equilibrium [Sa,V] is a thermal maximum, explained in detail in Peterson and Newton (1989) and Grant (1986). The sanidine-absent melting reaction [Sa] changes character at a singular point (S, insert) slightly higher in pressure than the six-phase invariant point (I) as the liquid increases in H_2O content.

in the systems K_2O-MgO-Al_2O_3-SiO_2-H_2O (KMASH) and KMASH-CO_2. The KMASH equilibria show a close approach to univariant behavior, and can be modeled in the quasi-four-component system $KAlO_2$-MgO-SiO_2-H_2O (Grant, 1986). The equilibria include an orthopyroxene-absent melting curve [En], a sanidine-absent melting curve [Sa], a phlogopite-absent melting curve [Ph], a vapor-absent melting curve [V], a subsolidus (liquid-absent) dehydration curve [L], and a univariant vapor-absent thermal maximum [Sa,V]. Not shown is a quartz-absent melting curve, because this study concentrates on quartz-present equilibria. The positions of the KMASH univariant curves in Figure 1 are as determined by Peterson and Newton (1989).

A univariant melting curve in the KMASH-CO_2 system, deduced by Wendlandt (1981), is expressed by the reaction

$$\underset{\text{phlogopite}}{KAlMg_3Si_3O_{10}(OH)_2} + \underset{\text{sanidine}}{KAlSi_3O_8} + \underset{\text{quartz}}{SiO_2} + \underset{\text{vapor}}{CO_2\text{-}H_2O} = \underset{\text{enstatite}}{MgSiO_3} + \underset{\text{liquid}}{\text{Si-melt}} \quad (1)$$

This equilibrium is the intersection in the P-T-vapor (CO_2-H_2O) space of divariant equilibria that emanate from the univariant KMASH curves in Figure 1. The P-T curve of Reaction 1 was located experimentally by Wendlandt; it lies at temperatures nearly as low as the vapor-saturated melting curve of phlogopite + potassium feldspar + quartz in the pure H_2O system. Moreover, addition of CO_2 to the KMASH system depresses the potassium feldspar–absent [Sa] solidus below the corresponding solidus in the CO_2-free H_2O-saturated system. These features contrast greatly with the behavior of CO_2 in simple quartz-feldspar systems without mafic components, where CO_2 markedly elevates the H_2O-saturated solidus (Holtz et al., 1988; Keppler, 1989).

Depression of the phlogopite + quartz melting point under elevated CO_2 pressures has an analogue in the lowering of the vapor-present melting point of pargasite by the addition of CO_2 to the H_2O vapor (Holloway, 1973). Between 2 and 7 kbar, the pargasite solidus is lowered 20–30 °C under the pure H_2O solidus in the presence of fluids with as much as 70% CO_2. The phenomenon of CO_2-enhanced melting may be a general property of hydrous silicates in mafic-alkaline systems. It is probable that Na_2O and FeO behave similarly to K_2O and MgO, respectively, during CO_2-enhanced melting.

The experiments of Wendlandt (1981) indicate that CO_2 may have a major bearing on the chemistry, solidus mineralogy, and origin of felsic silicate magmas. Charnockitic magmas (granitic or quartz syenitic liquids saturated with orthopyroxene) can exist at high-grade metamorphic conditions and thus may be anatectic in origin, as inferred by Wendlandt (1981) and Grant (1986). CO_2 infiltration into mid- and lower-crust rocks may promote migmatite formation, with orthopyroxene among the neosome assemblage. CO_2-rich solutions may be evolved in large quantities from some crystallizing charnockitic magmas, and these fluids may promote subsolidus recrystallization of adjacent rocks in the granulite facies (Frost and Frost, 1987).

Wendlandt's work, although far-reaching in its implications, has not gained widespread acceptance, in part because the data are of a preliminary nature. Compositions or descriptions of the quenched liquids encountered were not given, and no estimate was made of the compositions of the CO_2-H_2O fluids in equilibrium with liquids. The experiments were made with small amounts of oxalic acid dihydrate added to the charges, and it was assumed that the vapor and liquid compositions were buffered at the univariant equilibrium.

Our work reinvestigates melting of phlogopite, quartz, and sanidine in the KMASH-CO_2 system, with emphasis on the liquid compositions and the demonstration of chemical equilibrium by reversal experiments. These consist of demonstrating regrowth of subsolidus assemblages from the liquids at temperatures below observed melting points and of reversed determination of the fluid compositions in equilibrium with liquids along Reaction 1.

Experimental methods

Apparatus

Experiments were performed in internally heated gas vessels (design after Holloway, 1971) below 6 kbar, and in a piston-cylinder apparatus with a ¾-in. diameter pis-

TABLE 1. Constraining data for the [Sa] reaction phlogopite + quartz + vapor = enstatite + liquid, in the KMASH-CO_2 system

Experiment no.	Wt% vapor	P (kbar)	T (°C)	$X(H_2O)$ vapor initial	$X(H_2O)$ vapor final	Time (h)	Products
257	46	2.7	770	0.50	0.46	63	Qz + En + Gl + (Ph) + V
277	51	3.5	740	0.50	0.50	333	Ph + Qz + (En) + V
260	40	3.4	771	0.50	0.73	283	Qz + En + Gl + (Ph) + V
254	50	3.4	785	0.50	0.38	112	Qz + En + Gl + (m) + (Ph) + V
279	69	3.5	813	0.50	0.48	509	Qz + En + Gl + m + (Ph?) + V
266	50	3.4	850	0.50	0.49	238	En + Gl + (Qz) + V
267	37	3.5	785 → 740	0.50	0.49	283 → 221	Ph + Qz + (En) + V
255	49	6.0	763	0.50	0.53	111	Qz + En + qcl + Gl* + (Ph) + V
253	58	6.0	770	0.50	0.55	73	Qz + En + qcl + Gl* + V
275	48	6.0 → 3.5	770 → 783	0.50	0.51	73 → 162	Qz + En + Gl + (m?) + V

Note: Starting assemblage = Ph + Qz + V, Ph = phlogopite, Qz = quartz, Gl = glass, Gl* = glass only as inclusions, qcl = very fine-grained quenched melt material, En = enstatite, V = vapor, ? = presence of phase uncertain, ( ) = small to trace amount, m = quench mica, → = second stage of experiment.

ton using NaCl as pressure medium and graphite furnaces at pressures of 6 kbar and greater. Accuracy of pressure measurement was ±50 bars in the gas apparatus and ±200 bars in the piston cylinder. Temperatures were measured by chromel-alumel thermocouples and controlled automatically, with accuracies of ±5 °C for the gas apparatus and ±10° for the piston-cylinder apparatus.

Starting materials

Synthetic phlogopite, synthetic sanidine, and natural quartz were the same as in the KMASH study of phlogopite melting of Peterson and Newton (1989). The phlogopite was prepared hydrothermally from reagent MgO, K_2CO_3 or K_2NO_3, γ-Al_2O_3, and fused silica at 800 °C and 1 kbar for 10 d. Unit-cell constants of the phlogopite were somewhat variable in individual syntheses, with typical values of a = 5.299 Å, b = 9.218 Å, c = 10.327 Å and β = 99.84°. The phlogopite unit-cell constants were similar to those reported in previous studies of phlogopite melting (Wones and Dodge, 1977; Bohlen et al., 1983).

Starting materials were homogenized mixtures of phlogopite + quartz (2:3 by weight) and phlogopite + sanidine + quartz (2:2:3). The mixtures were sealed with various amounts of oxalic acid dihydrate, $(COOH)_2 \cdot 2H_2O$, and anhydrous oxalic acid, $(COOH)_2$, into Pt tubing with a diameter of 3 mm and a length of 1.5 cm.

Vapor-phase characteristics

Two kinds of experiments were conducted, one with very large amounts of oxalic acid (about equal to the weight of the solid charge), so that vapor composition was not changed appreciably during a melting or dehydration reaction, and another with smaller amounts of vapor in which changes in the ratio of CO_2 to H_2O could occur during a reaction. Capsules were checked for weight change after an experiment. The capsules remained constant in weight to within ±0.03%, indicating complete retention of the volatiles. Equilibrated vapor compositions were determined by a puncture weight-loss technique. Immediate weight loss upon puncture gave the CO_2 content, and weight loss after drying for half an hour at 110 °C gave the relative amount of H_2O present in the vapor.

Oxalic acid dihydrate in sealed Pt capsules should yield a vapor phase of equimolar H_2O and CO_2 as H_2 diffuses out of the capsule (Holloway and Reese, 1974), provided that graphite does not precipitate. An indication that the expected vapor compositions were maintained is shown by the vapor composition determinations of Table 1. Anhydrous oxalic acid yields a pure CO_2 vapor (Holloway and Reese, 1974) under moderately oxidizing conditions. Vapor compositions between $X^{Vap}_{H_2O} = 0.50$ and $X^{Vap}_{H_2O} = 0$ were generated with weighed mixtures of hydrous and anhydrous oxalic acid.

In some experiments with less than ~13 wt% vapor, large changes of the vapor composition were noted after an experiment. The direction of the change depended on the reaction that took place. H_2O was absorbed into a liquid or crystallizing phlogopite, CO_2 was absorbed into a liquid, or H_2O was released upon phlogopite dehydration. The measured vapor-phase composition is an indicator of subsolidus reaction (phlogopite breakdown or growth) but is somewhat less definitive in melt-field experiments because of possible failure to quench the equilibrium volatile content into a glass. This was particularly apparent in experiments above 3.5 kbar, where liquids could not be quenched to glasses and consequently must have released most of their volatiles to the vapor phase during the quench. At 2.5 kbar, the measured vapor phase appeared to be a reliable indicator of the nature and equilibrium vapor composition of a reaction.

Experiments below about 750 °C at 10 kbar and below 690 °C at 6–7 kbar contained variable amounts of a dispersed opaque phase, undoubtedly graphite. These experiments also showed some shifts of the vapor to more H_2O-rich compositions. This departure from intended vapor compositions presented a fundamental limitation to the study that might have been partially overcome with an oxidizing external buffer; however, encapsulated H_2O-bearing HM and NNO buffers in the piston-cylinder apparatus have lifetimes of only 24–48 h at temperatures near 700 °C (Ganguly and Newton, 1968). An attempt to

Table 2. Representative analyses of quenched melt from 3.4 kbar and 785 °C in equilibrium with quartz + enstatite + vapor ($X^{v}_{H_2O} = 0.50$)

Oxide wt%	1	2	3	4	5	6	7	8	
K_2O	3.98	4.36	5.16	5.00	3.62	3.73	2.90	3.42	5.81
SiO_2	35.26	43.76	46.85	31.62	36.55	35.69	27.78	36.52	61.99
MgO	13.37	13.70	15.36	16.73	13.83	13.33	12.67	13.79	23.41
Al_2O_3	5.82	6.04	8.02	6.51	5.36	5.24	4.91	5.18	8.79
Total	58.43	67.86	75.39	59.86	59.36	57.99	48.26	58.91	100

Note: Sample no. 254 analyzed on Cameca SX50 electron microprobe. Analyses 1–4 obtained using a WDS system with 10-kv accelerating voltage and 2-nA beam current. Analyses 5 and 6 obtained using a EDS system with 15-kv accelerating voltage and 5-nA beam current. Analyses 7 and 8 obtained using a EDS system with 15-kv accelerating voltage and 10-nA beam current. Numbers 1–6 = analyses of glass globules, numbers 7 and 8 = analyses of grain-boundary glass around quartz. Beam diameter was <1 μm for all operating conditions. Right-hand column of analysis no. 8 is renormalized to 100%.

increase the buffer size would result in additional temperature uncertainty in the experiment and would only marginally increase possible experiment times.

Chemical analysis

Analyses of quenched melt and enstatite were obtained with a Cameca SX50 electron microprobe and a JEOL scanning electron microscope with EDS analysis capabilities. Direct analysis of quenched melt was performed, as well as programmed linear scans at intervals of 5 μm across aggregates of products. Counting times were 30–60 s, with K_2O counts collected during the first 25% of counting time. Specific conditions of analysis are in Tables 2–4.

Optical identification

The most important identification technique was optical inspection of lightly crushed portions of the quenched charges in oil of refractive index 1.540. In this medium quartz has slightly positive relief, phlogopite moderately positive, enstatite highly positive, sanidine slightly negative, and glass markedly negative relief. Glass, representing quenched melt, was detectable in a number of forms. These included rounded globules of up to 50 μm in diameter, commonly with brightly birefringent margins (Fig. 2a), partially devitrified patches interstitial to radiating clusters of enstatite crystals (Fig. 2b), small (~5 μm) inclusions in enstatite (Fig. 2c) and quartz, and thin grain boundary partitions separating well-formed recrystallized quartz grains in aggregates. Commonly, trails of glass inclusions, some elongate, outlined quartz grain boundaries.

The globular shape of glass particles in the lower-temperature melting experiments below 6 kbar is reminiscent of quenched vapor precipitates in some higher-pressure experiments in hydrous silicate systems (e.g., albite-H_2O, Goldsmith and Jenkins, 1985). Several observations make this interpretation highly unlikely for these experiments. These include the mafic nature of the glass, identical analyses of globules and glass on quartz grain boundaries (Table 2), the very low vapor solubility of silicates in CO_2-bearing systems (Schneider and Eggler, 1986), and the glass inclusions in enstatite, which are consistent with the formation of enstatite by a melting reaction. A few slender inclusion-free needles of enstatite in experiments interpreted as subsolidus (e.g., no. 277, Table 1) result from the small incongruent vapor solubility of phlogopite.

Apparently, the liquids had the ability to promote substantial recrystallization of quartz. Large, euhedral quartz grains were abundant, which commonly included several dark quartz seed cores in syneusis texture. The presence of large recrystallized grains was a useful criterion in determining that melting had occurred in an experiment.

Large fragments or globules of glass were not observed at pressures above 3.5 kbar, though grain-boundary partitions in quartz aggregates and patches interstitial to radiating enstatite prisms were present. Thick mat-like clusters of acicular and dendritic phlogopite were present at the higher pressures (Fig. 2d). These patches were interpreted as quenched melt. Original phlogopite in the

Table 3. Representative analyses of quenched melt from 3.4 kbar and 850 °C in equilibrium with quartz + enstatite + vapor ($X^{v}_{H_2O} = 0.50$)

Oxide wt%	1	2	3	4	5	6	7	8	9	10
K_2O	5.85	6.67	7.70	5.64	6.31	6.14	6.71	6.61	6.06	6.51
SiO_2	77.60	75.90	78.28	72.99	77.52	75.50	76.37	69.23	73.95	71.53
MgO	5.28	6.38	1.56	11.23	5.16	8.08	5.33	3.42	1.94	0.49
Al_2O_3	11.27	11.05	12.45	10.14	11.01	10.28	11.59	9.89	11.40	11.40
Total			analyses normalized to 100%					89.15	93.35	89.93

Note: Sample no. 266. Analyses 1–7 obtained using a JEOL scanning electron microscope with an EDS system at 15-kv accelerating voltage and 200-pA beam current. Instrument returns normalized analyses. Analyses 8–10 obtained using a Cameca SX50 electron microprobe with WDS system at 10-kv accelerating voltage and 2-nA beam current.

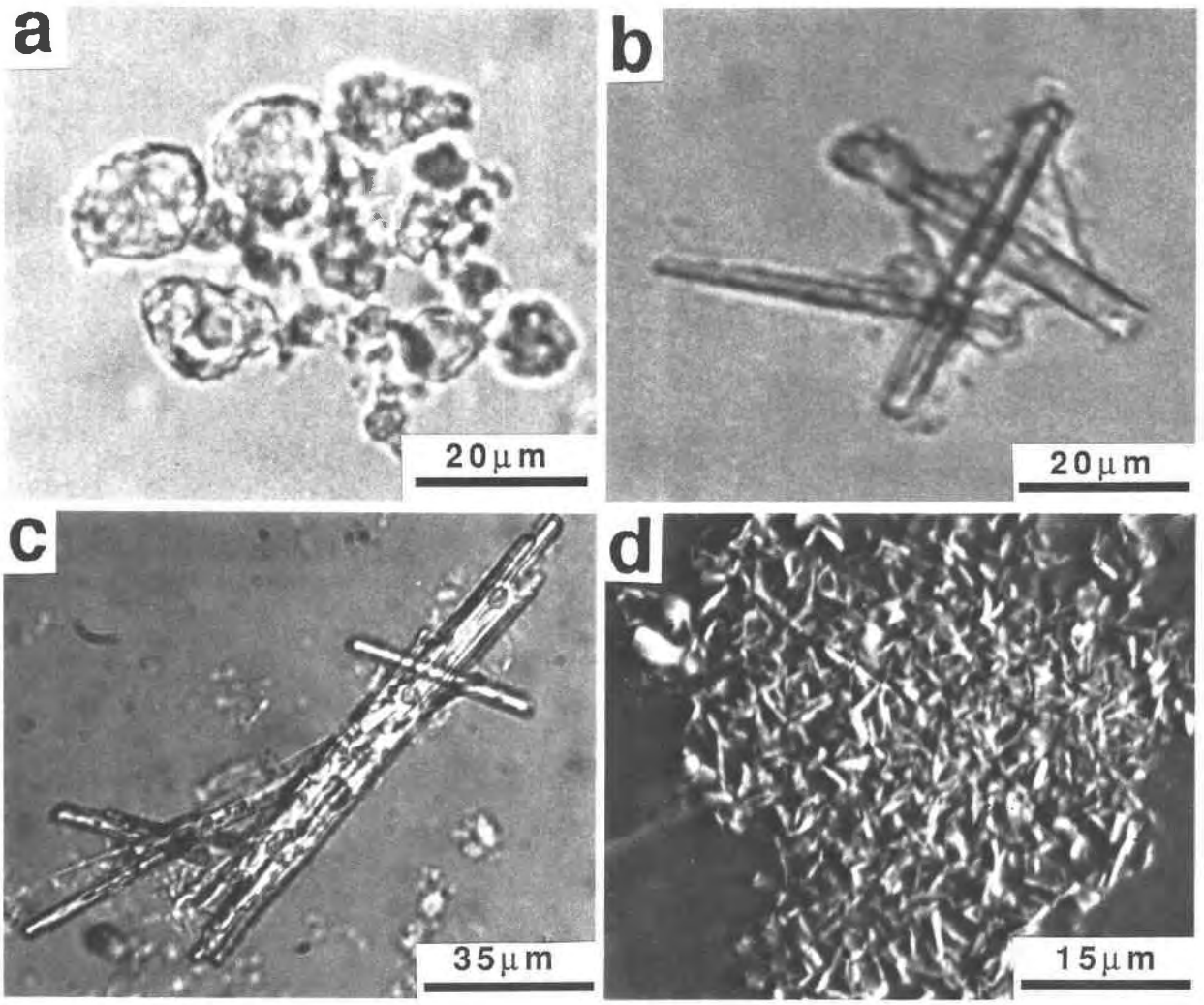

Fig. 2. (a) Ordinary light photomicrograph of glass globules quenched from experiment no. 254, Table 1 (Ph + Qz + excess equimolar CO_2-H_2O vapor, 3.4 kbar, 785 °C). (b) Ordinary light photomicrograph of enstatite produced in experiment no. 254, Table 1, showing partially devitrified interstitial glass. (c) Ordinary light photomicrograph of enstatite produced in experiment no. 254, Table 1, containing rounded glass (quenched melt) inclusions. (d) Scanning electron micrograph of matlike cluster of acicular and dendritic phlogopite and unidentified matrix material quenched from experiment no. 253, Table 1 (Ph + Qz + excess equimolar CO_2-H_2O vapor, 6.0 kbar, 770 °C). This texture is present in experiments above 3.5 kbar and is interpreted as quenched liquid.

Table 4. Representative analyses of quenched melt from 6 kbar and 770 °C in equilibrium with quartz + enstatite + vapor ($X^{Vap}_{H_2O} = 0.50$)

Oxide wt%	1		2		3		4	
K_2O	4.16	7.93	5.14	8.56	3.82	7.89	3.42	8.17
SiO_2	24.56	46.83	27.60	45.95	22.44	46.33	19.27	46.02
MgO	16.20	30.89	18.59	30.95	15.07	31.11	13.29	31.74
Al_2O_3	7.53	14.36	8.74	14.55	7.11	14.68	5.89	14.07
Total	52.45	100	60.07	100	48.44	100	41.87	100

Note: Sample no. 253 analyzed on Cameca SX50 electron microprobe with a EDS system, 15-kv accelerating voltage and 10-nA beam current. Analyses 1 and 2 obtained using a beam size of 1-μm diameter; 3 and 4 obtained using a beam size of 10-μm diameter.

starting material was identifiable as highly birefringent flakes randomly distributed with angular quartz and small sanidine grains. In some experiments, phlogopite recrystallized to very large (~50–100 μm) poikilitic crystals riddled with quartz, commonly having vague pseudohexagonal outlines (Fig. 3). When grown from liquid in reversal experiments, phlogopite commonly enclosed granular relics of large enstatite crystals.

Trapped vapor as fluid inclusions in quartz was commonly observed. Some of the inclusions were up to 30 μm across, and were generally two-phase, with a high-relief fluid, undoubtedly liquid CO_2, occupying the centers of rounded and tubular cavities, surrounded by an immiscible fluid, undoubtedly liquid H_2O, lining the cavity walls. Sometimes a small vapor bubble in rapid motion was present in the CO_2 area. This vapor could not be homogenized with conoscopic light, and thus was not gaseous CO_2. Fluid inclusions often occurred side by side with glass inclusions in quartz. The fluid inclusions sometimes contained tiny specks of condensed material, probably less than a tenth of a percent by volume. The small amount of precipitate in the fluid inclusions shows that critical mixing between liquid and vapor is not closely approached in the pressure range below 10 kbar.

Reversal criteria

Two kinds of reversal experiments were attempted. In one, the composition of the vapor in equilibrium with the assemblage phlogopite + sanidine + quartz + enstatite + liquid was constrained by changes from starting compositions in experiments of 6–13 wt% total volatiles. In the other kind of reversal experiment, phlogopite was regrown from liquid and enstatite, as indicated by the presence of large poikilitic phlogopite crystals having pseudohexagonal morphology with granular enstatite cores (Fig. 3). These reversal experiments were performed in two-stage experiments. In the first stage, a capsule containing starting materials and excess vapor of equimolar composition was held at a P and T determined to produce melting in a previous experiment for an equivalent length of time. Next, the temperature of the same experiment was lowered isobarically to a temperature at which no melting had occurred in a previous experiment, and held at that temperature for a duration about equal to that of the first stage.

Results of experiments

Reaction: phlogopite + quartz + vapor = enstatite + liquid

Experimental data for the sanidine-absent reaction [Sa] are in Table 1. At 3.4–3.5 kbar quenched liquid was present as discrete glass globules, grain-boundary linings, inclusions in enstatite prisms and quartz grains, and rarely as masses of phlogopite quench crystals. Melting occurred at 771 °C but not at 740 °C in the presence of a vapor composition of $X_{H_2O} = 0.50$.

Melting was reversed in a two-stage experiment (no. 267, Table 1). A charge of phlogopite, quartz, and excess oxalic acid dihydrate was held at 785 °C for 283 h, sufficient for nearly complete melting of phlogopite, as indicated by the results of experiment no. 254, Table 1. The temperature was then lowered in the same experiment to 740 °C and held for 221 h. The nature of phlogopite regrowth around enstatite cores is pictured in Figure 3. All glass disappeared in this experiment. The data of Table 1 constrain the melting of phlogopite + quartz + vapor $(CO_2)_{0.5}(H_2O)_{0.5}$ to 755 ± 15 °C at 3.4–3.5 kbar, as shown by the dashed bracket in Figure 4.

Melting of phlogopite + quartz + vapor of composition $X^{Vap}_{H_2O} = 0.50$ occurs at temperatures as low as 763 °C at 6 kbar, as deduced by the presence of very fine-grained phlogopite mats, thin grain-boundary glass linings in quartz aggregates, and large, euhedrally recrystallized quartz grains. We did not attempt to reverse the melting at pressures above 3.5 kbar. Therefore, the $(CO_2)_{0.5}(H_2O)_{0.5}$ vapor contour on the phlogopite + quartz + enstatite + liquid + vapor surface is unconstrained above that pressure. The principal conclusion, however, is that CO_2-H_2O mixtures lower the melting point of phlogopite + quartz by at least 30 °C below the melting point in the H_2O-saturated CO_2-absent KMASH system determined by Peterson and Newton (1989).

Compositions of glass globules and glass linings on quartz grains from an experiment at 3.4 kbar and 785 °C are in Table 2. The microprobe totals are very low in these experiments and quite variable. These decrements result from the high volatile content of the glasses, though they probably do not record the true volatile contents. Other causes of low totals are poorly polished surfaces of microvesicular or friable glass and loss of K_2O from volatile-rich glass upon electron beam analysis.

Glass compositions are close to those on the join phlogopite-quartz. If it is assumed that K_2O and Al_2O_3 are equimolar in all phases (sanidine, phlogopite, and liquid), the compositions may be plotted in the $KAlO_2$-SiO_2-MgO triangle (Fig. 5). As a supplement to the glass analyses, a traverse was made across the entire polished product of experiment no. 254. Analyses of 30-s counts were made at 5-μm intervals. The results are plotted in Figure 5. A variety of compositions were encountered randomly. Almost all of the analyses are near the phlogopite-quartz join. A few analyses very close to enstatite composition were encountered. No analyses corresponding to sanidine were found in any of the experiments on the melting of phlogopite + quartz. The distribution is that of some mechanical mixture with overlapping analyses of quartz and phlogopite, or quenched liquid phase (glass and quenched-phlogopitic mats), or both. Two features indicate that the analyses represent a mixture of quartz and quenched melt. First, individual nondendritic (primary) flakes of phlogopite are rare in the charge, and second, there is a cutoff in the trend of the analyses that coincides nearly with the individual analyses of the glass globules. None of the analyses closely approaches phlogopite composition. The analyses thus reveal that the sample was largely molten and in the field of melt + quartz + ensta-

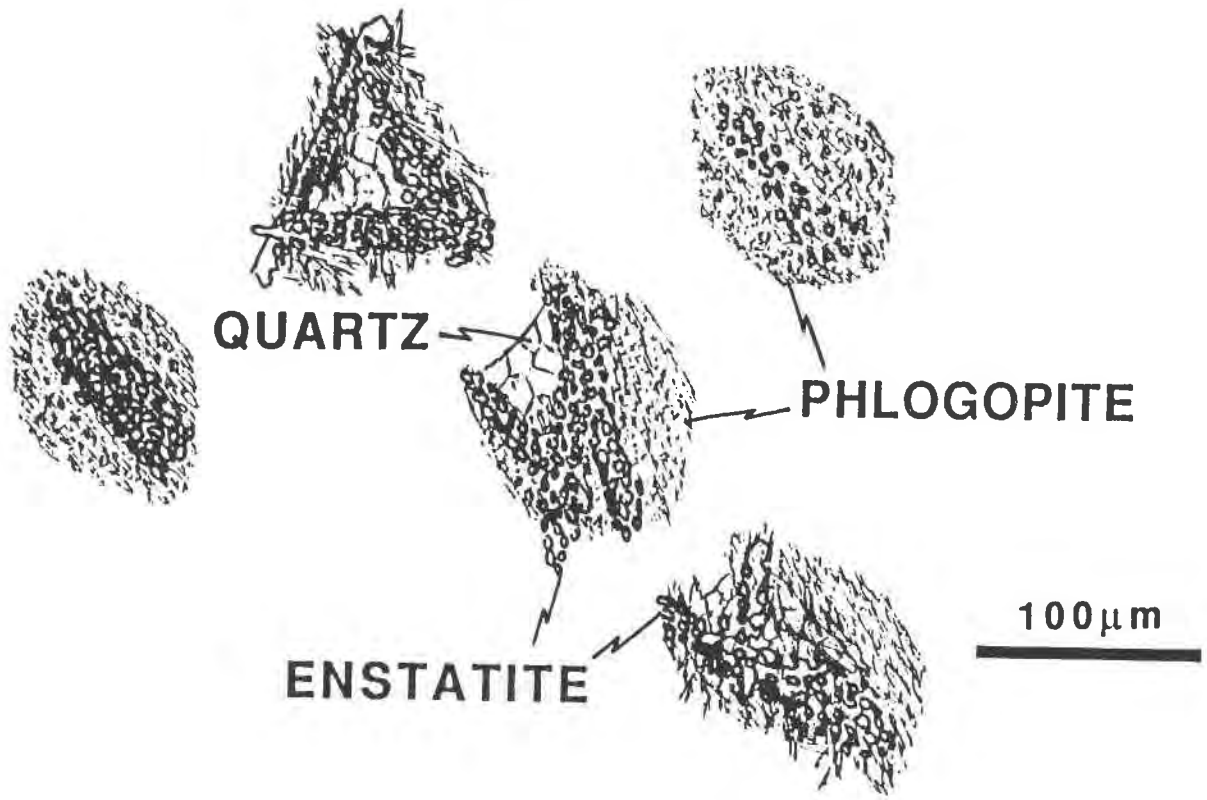

Fig. 3. Sketch of large poikilitic crystals of phlogopite enclosing granular relics of large enstatite crystals. Phlogopite crystals were grown in reversal at 740 °C and 3.5 kbar of melting equilibrium Ph + Qz + vapor $(CO_2)_{0.5}(H_2O)_{0.5}$ = En + L (experiment no. 267, Table 1).

tite. Sanidine is not a product of the melting reaction, as is true of the analogous KMASH reaction in the CO_2-absent system. The melt composition is mafic, with about 60% SiO_2 on a volatile-free basis and as much as 25% MgO.

An experiment on phlogopite + quartz + vapor (X_{H_2O} = 0.50) at 3.4 kbar and 850 °C (no. 266, Table 1) yielded glass + orthopyroxene + quartz. Quartz was much less abundant than in the experiment at 785 °C and the same pressure, and enstatite was more abundant. Glass analyses from the experiment at 850 °C are in Table 3. Glass was intimately mixed with small euhedral quartz grains and between rosettes of enstatite prisms and was difficult to analyze discretely. Figure 5 shows an analysis traverse of the experiment at 850 °C. The trend is slightly displaced toward the sanidine composition from the phlogopite-quartz join and shows a cutoff which is richer in SiO_2 than in the trend at 785 °C, consistent with the smaller amount of quartz in the experimental products. There is also the peculiar phenomenon of a sharp bend in the trend at 850 °C, with a segment that goes diametrically away from enstatite toward a point close to the KMASH sanidine-quartz melt composition (Peterson and Newton, 1989).

It is clear that most of the analyses are those of unresolved mixtures of quenched melt and quartz, and not of phlogopite and quartz, because of the cutoff in the trend (no analyses approached phlogopite closely). No significant overlap with enstatite is apparent. We suggest that the portion of the trend directed away from enstatite composition represents analyses of quenched melt of variable composition uncontaminated by quartz. This variation in composition could result from initial metastability of liquids, perhaps because of delayed enstatite nucleation, or from quench-precipitation of enstatite from the melts.

Table 4 presents analyses of the inferred quenched-melt phase from an experiment at 6 kbar and 770 °C. The totals are very low and variable, with lowest totals for the wide (10 μm) beam analysis, which suggests that the poorly polished surface inhibits reliable analysis.

Reaction: Phlogopite + quartz + sanidine + vapor = liquid

This reaction was investigated in the pressure range 1.9–10 kbar with large amounts of an equimolar H_2O-CO_2 vapor phase of constant composition. Experimental data are given in Table 5 and results illustrated in Figure 6. The open symbols denote experiments in which abundant melting occurred, represented in the quenched

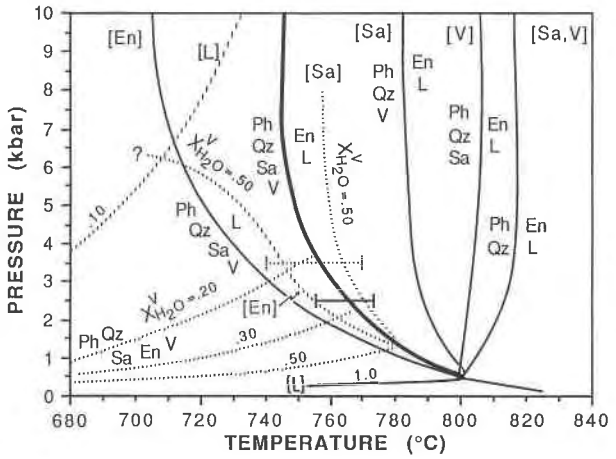

Fig. 4. Univariant equilibria in the KMASH and KMASH-CO_2 systems. A few contours (dashed) of constant H_2O mole fraction in vapor coexisting with [Sa], [En], and [L] assemblages are shown. These contours intersect in the six-phase univariant curve (bold line) from Wendlandt (1981). Solid bracket shows reversal interval of the six-phase equilibrium at 2.5 kbar. Dashed bracket encloses reversal interval for [Sa] equilibrium for vapor of composition $(CO_2)_{0.5}(H_2O)_{0.5}$. The [Sa] reaction (dashed curve) for $X^{V}_{H_2O} = 0.50$ may be at lower temperatures than illustrated at pressures above 3.5 kbar (cf. Fig. 8). The crossover of the [En] contours for equimolar vapor and pure H_2O vapor, requiring a temperature minimum in the [En] surface, is suggested but not proven. Contours of [L] calculated from the data set of Berman et al. (1985) with MRK CO_2-H_2O vapor (Kerrick and Jacobs, 1981).

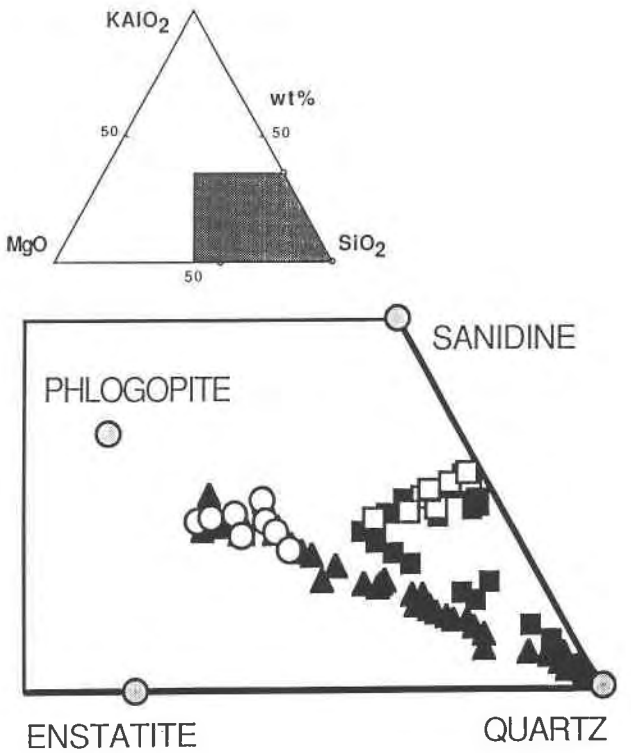

Fig. 5. Nonvolatile plot of quantitative analyses of products from H_2O-CO_2 experiments: open circles = quenched melt (glass) from 3.4 kbar and 785 °C (experiment no. 254, Table 1), open squares = quenched melt from 3.4 kbar and 850 °C (experiment no. 266, Table 1), filled triangles = random sampling of aggregate of products from 3.4 kbar and 785 °C (experiment no. 254), filled squares = random sampling of aggregate of products from 3.4 kbar and 850 °C (experiment no. 266). Enstatite analyses obtained during random sampling have been omitted. Trends of random analyses close to the phlogopite-quartz join are attributed to overlap of quenched melt and quartz. Trends of glass analyses and random analyses of experiment no. 266 near the join between enstatite and the KMASH sanidine-quartz eutectic may reflect metastable liquid compositions or variable amounts of enstatite crystallization in the quench (see text).

charges by dendritic phlogopitic quench-mats or by glass at quartz grain boundaries or in inclusions. The equimolar CO_2-H_2O results are surprising in that melting takes place at pressures above 6 kbar at temperatures as low as, or even lower than, in the pure H_2O (KMASH) system, shown by the dashed curve in Figure 6. If there is indeed a crossover of KMASH and KMASH-CO_2 melting curves, there exists a CO_2-rich residua subsystem involving the phases liquid + phlogopite + sanidine + quartz + vapor, with a melting minimum on the [En] vapor-composition surface, a feature not anticipated by Wendlandt (1981). We observed some evidence for melting in experiments down to 670 °C at 6–7 kbar. These experiments yielded carbon in the quenched charges and, accordingly, their interpretation is ambiguous.

Reaction: Phlogopite + quartz + sanidine + vapor = enstatite + liquid

Reaction 1 was investigated at 2.5 kbar with a starting assemblage of phlogopite + quartz + sanidine and small amounts of oxalic acids, which allowed changes of the vapor composition. These changes, together with the phase assemblages formed, constrain the T-X_{H_2O} location of the isobaric invariant point, satisfying some of the criteria of reversed equilibrium. Pertinent experiments are listed in Table 6 and plotted in Figure 7. The changes in vapor composition, along with the phase assemblages formed, constrain the isobaric six-phase invariant point to the lined rectangle, enclosed by temperatures of 773 °C and 757 °C and by vapor compositions of $X_{H_2O} = 0.39$ and 0.27. The uncertainties in these compositions may be estimated as the mean-root-squared deviation of vapor determinations from the expected composition of $X_{H_2O} = 0.5$ in Table 1, which gives ±0.09. As an example of the logic of the diagram, consider experiment no. 268, Table 6, in which an initial vapor of $X_{H_2O} = 0.30$ changed to 0.14 with the production of orthopyroxene and liquid (identified by glass) at 773 °C. The small amount of phlogopite in the charge is interpreted as incompletely reacted, because the final vapor composition is too CO_2-rich to be buffered at the six-phase invariant point and is

more probably fixed at the [Ph] reaction boundary. This interpretation puts an upper temperature limit of 773 °C on the invariant point. Similarly, experiment no. 2452 at 757 °C, which started with the vapor composition X_{H_2O} = 0.25 and which yielded orthopyroxene and did not melt, must lie below the invariant point in temperature. The negligible shift in vapor composition suggests that this experiment was buffered on the [L] reaction.

The experiments at 2.5 kbar confirm the existence of the six-phase Reaction 1 as deduced by Wendlandt (1981) (Fig. 4). The temperature of this equilibrium at 2.5 kbar corresponds closely to his placement of the curve. Our data add a new constraint to Reaction 1, which is the vapor composition of the six-phase assemblage. As will be shown, the experimentally determined composition is consistent with estimates based on thermodynamic data for the subsolidus assemblage phlogopite + orthopyroxene + sanidine + quartz + vapor.

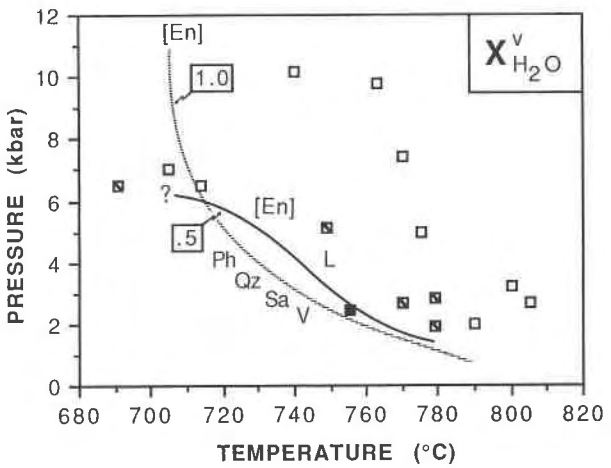

Fig. 6. *P-T* plot of experimental results on the [En] reaction phlogopite + quartz + sanidine + vapor $(CO_2)_{0.5}(H_2O)_{0.5}$ (Table 5). Open squares = definitive evidence for melting, slashed squares = only traces of glass or fine-grained micaceous quenched melt material present, filled square = inferred subsolidus conditions consistent with data from 2.5 kbar (Table 6 and Fig. 7). The [En] melting curves for pure H_2O and equimolar vapor compositions with their possible crossover are from Figure 4.

Discussion

P-T projection and solidus minimum

Figure 4 shows the *P-T* projections of the univariant curves and of a few contours of constant X_{H_2O} on the [Sa] and [En] and [L] vapor-composition surfaces. The X_{H_2O} = 0.50 contour on the [En] surface shifts to low temperatures in the range 3–6 kbar and may actually pass below the X_{CO_2} = 0 (pure H_2O) contour, which would thus indicate a minimum on this surface. The large depression of the solidus for mixed CO_2-H_2O fluids indicates that CO_2 becomes more soluble in KMASH liquids at pressures above approximately 3 kbar. Since CO_2 has only small solubility in simple model granites without mafic components in this *P-T* range, the increase in solubility with pressure in our work may result from a melt interaction with MgO, possibly as an $MgCO_3$ complex. The sudden onset of high CO_2 solubility between 3 and 6 kbar possibly results from the pressure control of a carbonation reaction in the liquid, analogous to magnesite stabilization in subsolidus assemblages.

Some estimate of the volatile composition and volatile content of the liquids formed in the [Sa] reaction may be determined from the glass analyses of experiment no. 254

Table 5. Constraining data for the [En] reaction phlogopite + quartz + sanidine + vapor = liquid, in the KMASH-CO_2 system

Experiment no.	Wt% vapor	*P* (kbar)	*T* (°C)	$X(H_2O)$ vapor initial	$X(H_2O)$ vapor final	Time (h)	Products
222	40	1.9	779	0.50	0.50	78	Ph + Qz + Sa + V + (Gl?)
232	29	2.0	790	0.50	0.56	217	Ph + Qz + Sa + qcl + V
233	50	2.7	770	0.50	0.50	375	Ph + Qz + Sa + (qcl?) + V
224	52	2.8	779	0.50	0.50	95	Ph + Qz + Sa + (qcl?) + V
230	40	2.7	805	0.50	0.45	103	Ph + Qz + Sa + qcl + (Gl) + V
236	49	3.2	800	0.50	0.50	173	Ph + Qz + Sa + qcl + m + V
123	30	5.1	749	0.50	?	256	Ph + Qz + Sa + V + (Gl?)
129	30	5.0	775	0.50	?	540	Qz + qcl + Gl + m + V
160	50	6.5	691	0.50	0.36	48	Ph + Qz + Sa + qcl + (Gl) + (m) + V
162	50	6.5	714	0.50	0.48	52	Ph + Qz + Sa + qcl + (Gl?) + (m?) + V
166	40	7.0	705	0.50	0.46	141	Qz + Sa + Gl + qcl + (m?) + V
2441	10.9	7.0	740	0.50	0.59	341	Ph + Qz + Sa + Gl + m + qcl? + V
247	11.0	7.2	750	0.50	0.57	548	Qz + (Sa) + Gl + m + V
2431	14.6	7.0	760	0.50	0.46	352	Qz + (Sa) + Gl + m + qcl? + V
231	62	7.4	770	0.50	0.55	47	Qz + Sa + qcl + m + V
161*	50	10.0	673	0.50	0.55	50	Qz + qcl + (Gl) + m + V
127*	30	10.2	740	0.50	?	91	Qz + Gl + qcl + m + (Sa?) + V
126*	30	9.8	763	0.50	?	67	(Ph) + Qz + (Sa?) + qcl + m + (En?) + V
165*	50	10.0	710 → 671	0.50	0.52	66 → 222	Qz + Sa + Ph? + qcl + Gl? + m + V

Note: Starting assemblage = Ph + Qz + Sa + V, Ph = phlogopite, Qz = quartz, Sa = sanidine, Gl = glass, V = vapor, En = enstatite, qcl = very fine-grained quenched melt material, m = quench mica, ? = presence of phase uncertain, ( ) = small to trace amount, → = second stage of experiment, * = small amount of graphite present in products.

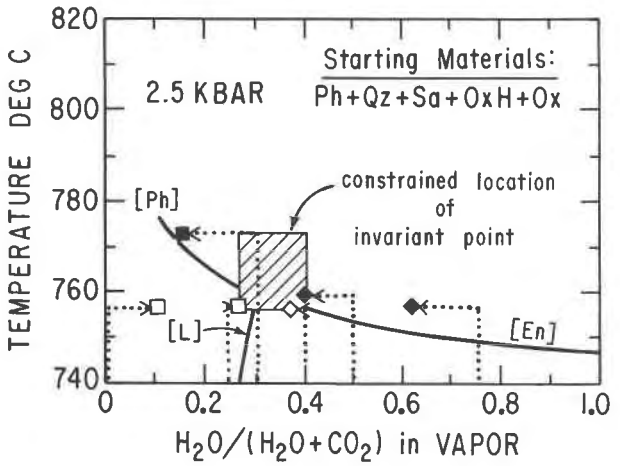

Fig. 7. Isobaric T-$X^{V}_{H_2O}$ plot of experimental data (Table 6) constraining location of six-phase invariant point at 2.5 kbar. Paths of arrows indicate initial and final compositions of vapor phase. Filled symbols = experiments in which melting occurred. Diamond symbols = experiments constraining [En] reaction. Square symbols = experiments constraining [Ph] reaction. OxH = oxalic acid dihydrate. Ox = anhydrous oxalic acid.

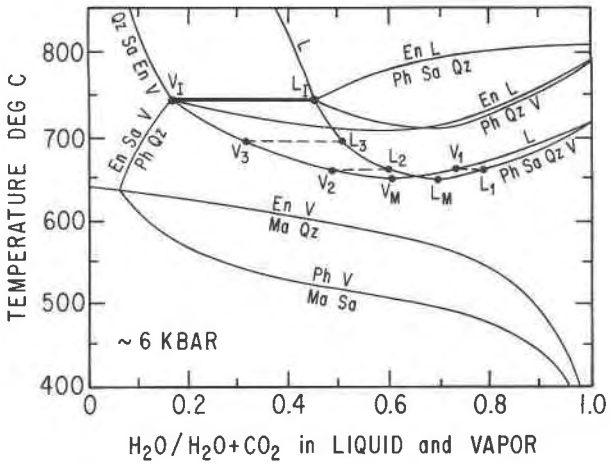

Fig. 8. Temperature vs. projected molar $H_2O/(CO_2 + H_2O)$ ratios of liquids and vapors at 6 kbar. Bold horizontal line is projection of isobaric invariant six-phase assemblage. Subsolidus equilibria are calculated from thermodynamic data (see text). Melting equilibria [En] and [Sa] may have minima near X_{H_2O} (vapor) = 0.6. A few tie lines of volatile ratios in coexisting vapor and liquid shown (V_1-L_1, etc.). Ma = magnesite, other abbreviations same as in previous diagrams.

at 785 °C and 3.4 kbar. Assuming that analysis no. 3, Table 2, with a probe total of 75.4%, is indicative, the total volatile content of the quenched liquid is 24.6 wt%. Assuming also that CO_2 enters the liquid as the $MgCO_3$ molecule, 16.9 wt% could be CO_2. If the remainder is H_2O, a molar $CO_2/(CO_2 + H_2O)$ value of 0.47 is indicated. This fulfills the expectation that the liquid volatile ratio is near, but somewhat less than, 0.5. An independent measurement, such as by infrared absorption, is needed to verify the postulated high carbonate content of the quenched glass. A similar estimate for the devitrified quenched melt of the experiment at 6 kbar, 770 °C (no. 253) based on analysis no. 2, Table 4, gives $CO_2/(CO_2 + H_2O)$ (liquid) = 0.30. This is undoubtedly a lower limit, since CO_2 escapes quantitatively in devitrification to phlogopite.

Our data do not define the behavior of the [Sa] surface. Since this reaction is chemically similar to the [En] reaction in the KMASH system, it is possible that the [Sa] surface shows a minimum, although it would have to be shallower than a minimum on the [En] surface.

Figure 4 shows a few X_{H_2O} (vapor) contours on the subsolidus surface [L], expressed by the reaction:

$$\underset{\text{phlogopite}}{KAlMg_3Si_3O_{10}(OH)_2} + \underset{\text{quartz}}{3SiO_2} = \underset{\text{enstatite}}{3MgSiO_3} + \underset{\text{sanidine}}{KAlSi_3O_8} + H_2O \quad (2)$$

The contours were calculated by use of the internally consistent data set of Berman et al. (1985), fugacity coefficients of H_2O in CO_2-H_2O mixes from Kerrick and Jacobs (1981), and thermal expansivities and compressibilities of the solid phases from Holland and Powell (1985). These parameters yield an end-member KMASH [L] curve, which agrees with the experimental work of Peterson and

Table 6. Constraining data for the six-phase invariant point phlogopite + quartz + sanidine + enstatite + liquid + vapor at 2.5 kbar

Experiment no.	Wt% vapor	T (°C)	$X(H_2O)$ vapor initial	$X(H_2O)$ vapor final	Time (h)	Products
2482	11.7	757	0.0	0.10	486	Qz + En + Sa + V
2452	9.7	757	0.25	0.27	508	Qz + Ph + En + Sa + V
2491	7.3	756	0.39	0.38	477	Qz + Ph + Sa + V + Gl?
2483	12.9	757	0.75	0.61	486	Qz + Sa + V + Gl + m
241	10.4	760	0.50	0.40	290	Qz + Sa + V + Gl + (En) + Ph? + m?
268	9.4	773	0.30	0.14	429	Qz + Ph + En + Sa + V + Gl
240	10.7	782	0.50	0.41	341	Qz + Sa + V + Gl + m

Note: Starting assemblage = Ph + Qz + Sa + V, Ph = phlogopite, Qz = quartz, Sa = sanidine, Gl = glass, V = vapor, En = enstatite, ? = presence of phase uncertain, ( ) = small to trace amount, m = quench mica.

Newton (1989). The vapor composition deduced experimentally for the six-phase assemblage at 2.5 kbar, $X_{H_2O}^{Vap} = 0.27–0.39$, is supported by the calculated vapor compositions. A significant feature of the calculations is that very CO_2-rich vapors produce melting of phlogopite + quartz + sanidine assemblages according to Reaction 1 at pressures above 5 kbar.

T-X_{H_2O} projection

Figure 8 is a semiquantitative depiction of the equilibrium relations at 6 kbar. The traces of the vapor and liquid composition surfaces intersect in Reaction 1, which is invariant at constant pressure. The isobaric invariant vapor and liquid $H_2O/(H_2O + CO_2)$ ratios are labeled, respectively, V_1 and L_1. The trace of vapor compositions of the [L] reaction as a function of temperature, calculated from the Berman et al. (1985) data set, is shown in Figure 8. Also shown are 6 kbar T-X_{CO_2} curves for the subsolidus equilibria:

$$\underset{\text{magnesite}}{MgCO_3} + \underset{\text{quartz}}{SiO_2} = \underset{\text{enstatite}}{MgSiO_3} + CO_2 \quad (3)$$

and

$$3\underset{\text{magnesite}}{MgCO_3} + \underset{\text{sanidine}}{KAlSi_3O_8} + H_2O = \underset{\text{phlogopite}}{KAlMg_3Si_3O_{10}(OH)_2} + 3CO_2 \quad (4)$$

calculated from the Berman et al. (1985) data set with updated parameters for magnesite from Chernosky and Berman (1989).

The hypothetical minimum in the [En] reaction is somewhat arbitrarily set at X_{H_2O} (vapor) ≈ 0.6 (point V_M). The volatile ratio L_M in the hypothetical minimum liquid is presumed to be somewhat greater than 0.6. Isothermal vapor-liquid tie lines are designated V_1-L_1, etc. A shallow minimum in the [Sa] surface is suggested also. The [V] surface extends from about 805 °C for the pure H_2O system to the isobaric invariant temperature of 745 °C at 6 kbar given by Wendlandt (1981), which we assume is correct. We have verified his placement of Reaction 1 only at 2.5 kbar.

The large depression in temperature of the [En] surface for $X_{CO_2} = 0.5$ between 3 and 6 kbar can be understood from the disposition of subsolidus curves in Figure 8. The proximity of the subsolidus decarbonation curves to the hypothetical melting minimum is consistent with the concept that increasing pressure stabilizes a carbonate molecule within the liquid, thus allowing high CO_2 solubility. Because of the relaxed structural requirements of a liquid in comparison to a crystalline carbonate, the pressure threshold of carbonate stability in the liquid is slightly lower than that of subsolidus magnesite stability with sanidine and quartz. An analogous anticipation effect occurs in the solidus of the peridotite-CO_2 system, which shows a sudden drop in temperature at about 20 kbar, anticipating the intersection of the dolomite and magnesite subsolidus stability curves (Wyllie and Huang, 1976). It is possible that at some higher pressure the magnesite stability curves in the present system actually intersect the solidus, so that magnesite precipitates from liquids along with phlogopite, sanidine, and quartz. Wendlandt (1981) reported magnesite in some products from experiments at pressures above 15 kbar.

Possible metastability of liquids

The trend of analyses of the experiment at 3.4 kbar and 850 °C shown in Figure 5 is approximately colinear with the enstatite composition. This trend could be explained by any of at least three different hypotheses: (1) Liquid compositions formed by phlogopite-quartz melting at 850 °C and 3.5 kbar are initially metastably enriched in MgO because of delayed nucleation and growth of enstatite. Initial melt compositions are close to the phlogopite-quartz join. With time enstatite forms, and the liquid moves diametrically away from enstatite toward the sanidine-quartz join. (2) Melt compositions are initially metastably impoverished in MgO, and enstatite formed early is partly metastable. With time the excess enstatite is resorbed and the liquid moves toward enstatite. (3) Enstatite is formed in the quench from MgO-rich, CO_2-rich liquids. The rosette texture of enstatite in experiments above 800 °C at 3.5 kbar may be evidence for this process. At present we cannot decide which of these mechanisms, if any, explains the curious linear trend of the 850 °C glass in Figure 5. That a majority of the quenched melt is near the phlogopite-quartz join is indicated by the frequently encountered hybrid analyses with quartz overlap, parallel to the trend for the experiment at 785 °C.

Hypothesis 2 is similar to the metastable melting of muscovite in a quartzofeldspathic rock at 1 kbar reported by Rubie and Brearley (1987). They found melting to a viscous silica-rich metastable liquid plus mullite or corundum, followed by eventual formation of more stable sillimanite-bearing assemblages. Some metastability of the liquids encountered in our study cannot be ruled out.

Isobaric sanidine- and quartz-present liquids

The liquidus surface for the KMASH-CO_2 system at constant pressure (about 6 kbar) with excess quartz and sanidine is shown somewhat speculatively on a triangular diagram with apices MgO, CO_2, and H_2O in Figure 9. The [Ph] and [En] polythermal cotectics are shown along with the vapor-absent liquid-crystal reaction curve [V]. The intersection of the isobaric univariant curves at L_1 is Reaction 1. In constructing this diagram, the projected molar compositions and the temperatures of the end-member KMASH curves were taken from Peterson and Newton (1989). The initial trend of the [En] curve into CO_2 space is based on the assumption that CO_2 and MgO enter the melt in equimolar amounts (i.e., as $MgCO_3$). Thus, the initial trend of the liquid away from the KMASH boundary is directly toward $MgCO_3$. Because of the linked high solubilities of MgO and CO_2, there is a

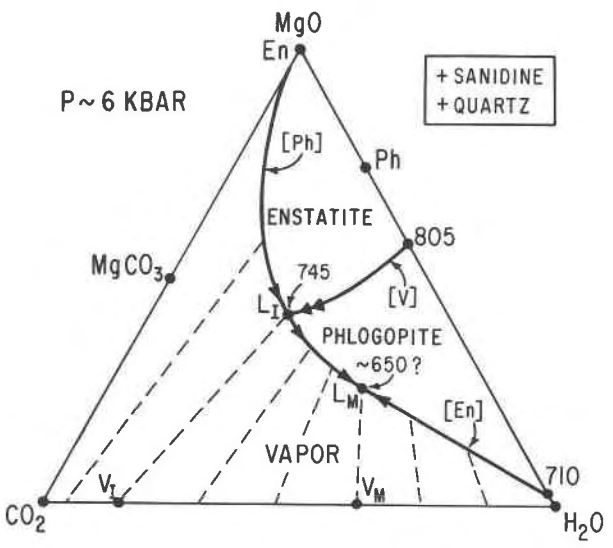

Fig. 9. Molar projection (from sanidine and quartz) at 6 kbar of compositions of liquids in equilibrium with [Ph], [En], and [V] assemblages. Vapor composition tie lines are schematic except for V_I, the equilibrium vapor of the isobaric invariant point (I), which was calculated from thermodynamic data, and V_M, which must be colinear with phlogopite and L_M, the composition of the hypothetical [En] minimum. Double arrow on [V] denotes crystal-liquid reaction. See text for further explanation. Abbreviations same as in previous figures.

lowering of the solidus. The figure suggests a minimum on the [En] cotectic; this is not yet proven. The minimum, L_M, would have to be colinear on this plot with the phlogopite composition, Ph, and the composition of the coexisting vapor, V_M. It is inferred that, after the hypothetical minimum has been achieved, there is a departure of the trend away from the CO_2 apex, as shown. This is because of the strong decarbonation tendency of the liquid with increasing temperature.

The location in Figure 9 of the six-phase invariant point is determined within certain limits by the following considerations. First, because enstatite was not encountered in experiments near 6 kbar on phlogopite + quartz + sanidine melting with excess oxalic acid dihydrate ($H_2O/CO_2 = 1/1$), the invariant liquid should lie to the left of the join MgO-$(CO_2)_{0.5}(H_2O)_{0.5}$. Second, from mass balance in the invariant reaction, which in projection is phlogopite + vapor (V_I) = enstatite + liquid (L_I), the invariant liquid must lie on the MgO-poor side of the join phlogopite-V_I. Finally, because of the decarbonation effect at higher temperatures along [En], the liquid compositions lie to the CO_2-poor side of the join [En] KMASH-$MgCO_3$. The invariant point I is plotted in the center of the triangle formed by these three lines, for lack of better definition.

The only constraint on the [Ph] equilibrium is that it must emanate from L_I and connect to a point on the MgO-CO_2 axis that is very close to MgO, considering that CO_2 solubility in high-temperature dry silicate liquids must be very small at pressures below 20 kbar. The [V] equilibrium beyond the MgO-H_2O sideline is similarly unconstrained; the line in Figure 9 suggests minimal curvature.

Geological applications

This study shows that CO_2 in felsic silicate liquids holds the mafic constituents in the liquid and delays crystallization of biotite. This principle would probably apply to amphibole as well. The accompanying depolymerization of the liquids with increased CO_2 content explains the inverse correlation of SiO_2 and mafic components in quartz syenites and charnockites noted by Wendlandt (1981). The analyses of some of the quenched melts from our experiments suggest that this principle may be extended to some of the lamprophyre clan rocks.

Granites and related lamprophyres

Many porphyritic granites, especially the anorogenic suite, contain a mafic-rich groundmass with abundant biotite (e.g., Anderson and Bender, 1989). The experimental results of this study indicate that the last liquids to freeze upon crystallization of granite in a CO_2-bearing system are rich in biotite components, in contrast to the behavior in many H_2O-rich felsic systems, where biotite is a phase that crystallizes early (Wyllie et al., 1976). Therefore, the texturally inferred position of biotite in the crystallization sequence of granitic rocks may reveal the compositional nature of the attendant fluid phase.

Further evidence for late-stage mafic liquids is the common association of lamprophyric dike rocks with granite plutons (Rock, 1987). The lamprophyre dikes commonly crosscut the granites. The mafic compositions of these dikes (suggesting mantle origin) have been difficult to reconcile with their great enrichment in incompatible elements (see Rock, 1987 and references therein). The compositions of some of the granite-associated lamprophyres, termed calc-alkaline lamprophyres, are tabulated by Bergman (1987). They are very similar to our analyses of experimental quenched liquids (Tables 2 and 4) in total mafic and alkali contents and commonly contain several percent of CO_2 as carbonate. In light of these observations, it is therefore distinctly possible that some of these dikes represent segregated late liquids accumulated in the crystallization of granite magmas that initially contained minor amounts of CO_2. If the minimum in the [En] curve shown in Figures 8 and 9 actually exists, and if there is an analogous minimum in more complex granitic systems, there would be a tendency for the liquid and the vapor to migrate toward the minimum. This tendency would be augmented if the vapor continually escapes rather than remains to react with the residual liquids.

A consequence of our work is that fluids with elevated CO_2 contents, perhaps sometimes approaching 30–40 mol%, might eventually evolve from initially CO_2-bearing granites. Such fluids may be important in mobiliza-

tion of hydrothermal ore deposits associated with felsic plutons.

Migmatites

The data presented in this study indicate that infiltration of CO_2-bearing fluids can produce partial melting in acid rocks. Depending on the CO_2-H_2O ratio of the fluid, the partial melt fraction would be more or less mafic, varying from granitic to lamprophyric. It is possible that biotite in some migmatites could have been a major component of a former interstitial liquid rather than a restite phase, as commonly supposed, if a CO_2-bearing vapor phase had been present.

If an infiltrating fluid were relatively rich in CO_2, perhaps initially on the CO_2-rich side of V_M (Fig. 9) the interstitial melt would be quite mafic. During freezing, the melt and the vapor would tend toward H_2O-richer compositions, but fluids given off in crystallization could be quite CO_2-rich. This may explain CO_2-rich fluid inclusions observed in the migmatites of the Front Range, Colorado (Olsen, 1987) or in the migmatites of the transitional granulite facies region of southern Norway (Touret and Dietvorst, 1983). Subsequent loss of H_2O from these inclusions, particularly after CO_2-H_2O immiscibility at lower temperatures, could have made the remaining inclusions even more CO_2-rich. The more traditional view of H_2O-rich granitic liquids gives no account of the migmatite CO_2-rich fluid inclusions, which would have to be incidental and not related to migmatite formation.

It seems possible from this study that orthopyroxene-bearing migmatites found in some granulite facies terranes, such as in southern Karnataka, India (Devaraju and Sadashivaiah, 1969), could have formed from infiltration of CO_2-rich fluids into felsic gneisses. Another possible mechanism is H_2O-undersaturated (i.e., vapor-absent) melting, as elegantly argued by Waters (1988) for the Namaqualand, South Africa migmatites. A problem raised by Waters is the small amount of hydrous alteration of the orthopyroxene; if the leucosomes were H_2O-rich granitic liquids, evolution of the H_2O in freezing should have altered the orthopyroxene to biotite. The relative lack of alteration could be explained by armoring of the orthopyroxene or strong channeling of the H_2O. Another possible explanation, based on the data of this study, is that CO_2-rich fluids were evolved by the liquids, which must have been more mafic and less SiO_2-rich than granitic liquids. Such fluids might have been in equilibrium with orthopyroxene as they were emitted.

Charnockite crystallization

A model KMASH charnockitic magma, with some CO_2 dissolved in it, crystallizing at a constant pressure of 6 kbar, would form biotite by reaction of orthopyroxene with liquid, either along the [V] reaction curve or at the invariant point L_1 (Fig. 9) at a temperature of about 745 °C. This is the final crystallization temperature of all charnockites that crystallized under equilibrium conditions to yield both orthopyroxene and biotite in the final assemblage, assuming the magma contained CO_2. Magmas with no CO_2 could crystallize completely under vapor-absent conditions to biotite-orthopyroxene rocks at 810 °C. Magmas would always eventually become vapor-saturated in the last stages if any CO_2 was present initially. If all orthopyroxene initially present reacts to form biotite, vapor and liquid compositions would tend toward the minimum at V_M and L_M, respectively.

Generation of charnockitic magmas by deep-crustal anatexis in a CO_2-rich environment is a possibility because of the relatively low temperatures required, as noted by Wendlandt (1981) and Grant (1986). Fluids in equilibrium with the magmas would be very CO_2-rich, with X_{CO_2} (vapor) of about 0.85 when biotite first crystallizes (Fig. 9). Liquids would tend toward granitic compositions in the evolution of these magmas and fluids associated with them would be progressively H_2O-rich. This could explain the succession of fluid inclusions found by Madsen (1977) in quartz in the composite charnockite-granite Kleivan pluton of southern Norway. The earlier charnockitic (orthopyroxene-bearing) portion of the pluton contains dominantly carbonic inclusions, whereas the later granitic (biotite-bearing) portion contains dominantly aqueous inclusions. The relatively small number of intermediate CO_2-H_2O inclusions could be explained by the tendency of H_2O to escape from mixed H_2O-CO_2 inclusions (Sterner et al., 1988).

Acknowledgments

The authors acknowledge valuable conversations with T. Chacko, B.R. Frost, J.A. Grant, W. Johannes, and P.J. Wyllie. We thank A.T. Anderson for his advice on fluid and melt inclusions in our experimental products and S.M. Kuehner for his analytical expertise. Reviews by S.R. Bohlen, J.A. Grant, and R.F. Wendlandt resulted in substantial improvement of the paper. This research was supported by NSF grant no. EAR 87-07156.

References cited

Anderson, J.L., and Bender, E.E. (1989) Nature and origin of Proterozoic A-type granitic magmatism in the southwestern United States of America. Lithos, 23, 19–52.

Bergman, S.C. (1987) Lamproites and other potassium-rich igneous rocks: A review of their occurrence, mineralogy and geochemistry. In J.G. Fitton and B.G.J. Upton, Eds., Alkaline igneous rocks. Geological Society Special Publication 30, 103–190.

Berman, R.G., Brown, T.H., and Greenwood, H.J. (1985) An internally consistent thermodynamic data base for minerals in the system Na_2O-K_2O-CaO-MgO-FeO-Fe_2O_3-Al_2O_3-SiO_2-TiO_2-H_2O-CO_2. Atomic Energy of Canada, Ltd., Technical Report TR-377, 1–62.

Bohlen, S.R., Boettcher, A.L., Wall, V.J., and Clemens, J.D. (1983) Stability of phlogopite-quartz and sanidine-quartz: A model for melting in the lower crust. Contributions to Mineralogy and Petrology, 83, 270–277.

Chernosky, J.V., and Berman, R.G. (1989) Experimental reversal of the equilibrium: Clinochlore + 2 magnesite + 3 forsterite + spinel + $2CO_2$ + $4H_2O$ and revised thermodynamic properties for magnesite. American Journal of Science, 289, 249–266.

Devaraju, T.C., and Sadashivaiah, M.S. (1969) The charnockites of Satnur-Halaguru area, Mysore State. Indian Mineralogist, 10, 67–88.

Frost, B.R., and Frost, C.D. (1987) CO_2, melts, and granulite metamorphism. Nature, 327, 503–506.

Ganguly, J., and Newton, R.C. (1968) Thermal stability of chloritoid at high pressure and relatively high oxygen fugacity. Journal of Petrology, 9, no. 3, 444–466.

Goldsmith, J.R., and Jenkins, D.M. (1985) The hydrothermal melting of low and high albite. American Mineralogist, 70, 924–933.

Goranson, R.W. (1938) Silicate-water systems: Phase equilibria in the $NaAlSi_3O_8$-H_2O and $KAlSi_3O_8$-H_2O systems at high temperatures and pressures. American Journal of Science, 35-A, 71–92.

Grant, J.A. (1986) Quartz-phlogopite-liquid equilibria and origins of charnockites. American Mineralogist, 71, 1071–1075.

Holland, T.J.B., and Powell, R. (1985) An internally consistent thermodynamic dataset with uncertainties and correlations: 2. Data and results. Journal of Metamorphic Geology, 3, 343–370.

Holloway, J.R. (1971) Internally heated pressure vessels. In G.C. Ulmer, Ed., Research techniques for high pressure and high temperature, p. 217–258. Springer-Verlag, New York.

——— (1973) The system pargasite-H_2O-CO_2: A model for melting of a hydrous mineral with a mixed-volatile fluid. I. Experimental results to 8 kbar. Geochimica et Cosmochimica Acta, 37, 651–666.

——— (1976) Fluids in the evolution of granitic magmas: Consequences of finite CO_2 solubility. Geological Society of America Bulletin, 87, 1515–1518.

Holloway, J.R., and Reese, R.L. (1974) The generation of N_2-CO_2-H_2O fluids for use in hydrothermal experimentation. I. Experimental method and equilibrium calculations in the C-O-H-N system. American Mineralogist, 59, 587–597.

Holtz, F., Ebadi, A., Barbey, P., Johannes, W., and Pichavant, M. (1988) Phase relations in the Qz-Ab-Or system at 2 and 5 kbar: The effect of a_{H_2O}. Terra Cognita, 8, 66.

Kadik, A.A., and Lukanin, O.A. (1973) The solubility-dependent behavior of water and carbon dioxide in magmatic processes. Geochemistry International, 10, 115–129.

Keppler, H. (1989) The influence of the fluid phase composition on the solidus temperatures in the haplogranite system $NaAlSi_3O_8$-$KAlSi_3O_8$-H_2O-CO_2. Contributions in Mineralogy and Petrology, 102, 321–327.

Kennedy, G.C., Wasserburg, G.J., Heard, H.C., and Newton, R.C. (1962) The upper three-phase region in the system SiO_2-H_2O. American Journal of Science, 260, 501–521.

Kerrick, D.M., and Jacobs, G.K. (1981) A modified Redlich-Kwong equation for H_2O, CO_2, and H_2O-CO_2 mixtures at elevated pressures and temperatures. American Journal of Science, 281, 735–767.

Le Breton, N., and Thompson, A.B. (1988) Fluid-absent (dehydration) melting of biotite in the early stages of anatexis. Contributions to Mineralogy and Petrology, 99, 226–237.

Madsen, J.K. (1977) Fluid inclusions in the Kleivan granite, South Norway, I: Microthermometry. American Journal of Science, 277, 673–696.

Novgorodov, P.G., and Shkodzinskiy, V.S. (1974) Experiments on melting of granite in H_2O-CO_2 mixtures and some problems of granite formation. Geochemistry International, 11, 522–531.

Olsen, S.N. (1987) The composition and role of the fluid in migmatites: A fluid inclusion study of the Front Range rocks. Contributions to Mineralogy and Petrology, 96, 104–120.

Peterson, J.W., and Newton, R.C. (1989) Reversed experiments on biotite-quartz-feldspar melting in the system KMASH: Implications for crustal anatexis. Journal of Geology, 97, 465–485.

Rock, N.M.S. (1987) The nature and origin of lamprophyres: An overview. In J.G. Fitton and B.G.J. Upton, Eds., Alkaline igneous rocks. Geological Society Special Publication 30, 191–226.

Rubie, D.C., and Brearley, A.J. (1987) Metastable melting during the breakdown of muscovite + quartz at 1 kbar. Bulletin de Minéralogie, 110, 533–549.

Schneider, M.E., and Eggler, D.H. (1986) Fluids in equilibrium with peridotite minerals: Implications for mantle metasomatism. Geochimica et Cosmochimica Acta, 50, 711–724.

Sterner, S.M., Hall, D.L., and Bodnar, R.J. (1988) Post-entrapment compositional changes in fluid inclusions: Experimental evidence for water diffusion in quartz. Geological Society of America Abstracts with Programs, 20, A100.

Touret, J., and Dietvorst, P. (1983) Fluid inclusions in high-grade anatectic metamorphites. Journal of Geological Society of London, 140, 635–649.

Tuttle, O.F., and Bowen, N.L. (1958) Origin of granite in the light of experimental studies in the system $NaAlSi_3O_8$-$KAlSi_3O_8$-SiO_2-H_2O. Geological Society of America Memoirs, 74, 1–153.

Vielzeuf, D., and Holloway, J.R. (1988) Experimental determination of the fluid-absent melting relations in the pelitic system. Contributions to Mineralogy and Petrology, 98, 257–276.

Waters, D.J. (1988) Partial melting and the formation of granulite facies assemblages in Namaqualand, South Africa. Journal of Metamorphic Geology, 6, 387–404.

Wendlandt, R.F. (1981) Influence of CO_2 on melting of model granulite facies assemblages: A model for the genesis of charnockite. American Mineralogist, 66, 1164–1174.

Wones, D.R., and Dodge, F.C.W. (1977) The stability of phlogopite in the presence of quartz and diopside. In D.G. Fraser, Ed., Thermodynamics in geology, p. 229–247. D. Reidel, Dordrecht, the Netherlands.

Wyllie, P.J. (1977) Crustal anatexis: An experimental review. Tectonophysics, 43, 41–71.

Wyllie, P.J., and Huang, W.-L. (1976) Carbonation and melting reactions in the system CaO-MgO-SiO_2-CO_2 at mantle pressures with geophysical and petrological applications. Contributions to Mineralogy and Petrology, 54, 79–107.

Wyllie, P.J., Huang, W.-L., Stern, C.R., and Maaløe, S. (1976) Granitic magmas: Possible and impossible sources, water contents, and crystallization sequences. Canadian Journal of Earth Sciences, 13, 1007–1019.

Manuscript received August 21, 1989
Manuscript accepted August 1, 1990